Pneumatic flow control studies using steady blowing on a supercritical aerofoil

C. Wong and K. Kontis
Aero-Physics Laboratory
School of Mechanical, Aerospace and Civil Engineering
University of Manchester
Manchester, UK

ABSTRACT

Experimental studies have been conducted on a NASA 17-percent thick supercritical aerofoil with a Coanda trailing edge at subsonic speeds in both the boundary-layer control and circulation control regimes. Detailed boundary-layer surveys were performed along the mid span on the suction surface and around the Coanda trailing edge. The wake located at 43% chord-length behind the aerofoil was measured with a single-component hotwire anemometer, and the profile drag coefficients were calculated from the integration of wake momentum deficit. Lift forces and pitching moments were recorded from –20deg to +20deg incidence using a 3-component force balance. In the circulation control regime, the boundary-layer results indicated that separation bubbles are not present at high incidences compared to the boundary-layer control regime, and that minimised the potential for flow separation delay around the Coanda trailing edge. The spectral analysis of the wake showed a significant reduction of wake fluctuations at high incidences and improvement of the stability at the edge of the wake. The study of aerodynamic forces suggested the need to increase the blowing momentum coefficient if the circulation control is used near the stalling angle-of-attack.

NOMENCLATURE

A_J	area of the jet slot
b	aerofoil span
c	aerofoil chord-length
C_d	drag coefficient
C_{dp}	profile drag coefficient
C_{dpc}	corrected profile drag coefficient due to blowing
C_{dEQUIV}	equivalent drag coefficient
C_l	lift coefficient
C_m	pitching moment coefficient
C_μ	blowing momentum coefficient
D_{dp}	profile drag
D_{EQUIV}	equivalent drag
D_{Power}	drag due to fluid power
D_{RAM}	momentum drag required to ingest the blowing flow rate
h	slot height
H_l	shape factor
L	lift
m	mass flow rate
p_s	static pressure
P_t	inlet pressure
q	dynamic pressure
r	radius of the trailing edge

Paper No. 3200. Manuscript received 16 April 2007, revised version received 15 October 2008, accepted 24 November 2008.

https://doi.org/10.1017/S0001924000002773 Published online by Cambridge University Press

S	wing area
u	velocity in streamwise direction
U_e	velocity at the edge of the boundary layer
U_J	jet velocity
U_o	velocity at the edge of wake
U_∞	freestream velocity
w	wake width
x	chordwise distance
y	vertical displacement
α	angle-of-attack, (AoA)
δ	boundary-layer thickness
δ^*	displacement thickness
ε	kinetic energy thickness
θ	momentum thickness
θ_A	angular position around the circular cylinder
θ_s	flow separation point around the circular cylinder
ρ_J	jet density
ρ_∞	freestream air density
CC	circulation control
BLC	boundary layer control

1.0 INTRODUCTION

Circulation control technologies have been developed since the early 1930s and have been successfully demonstrated under laboratory conditions and in flight vehicle demonstrations[1]. They are generally related to the pneumatic devices which are installed near the rear portion of an aerofoil. These devices can be categorised into jet flaps or blown flaps. A jet sheet exits from the trailing edge of the aerofoil at a fixed angle or tangent to a flap with a sharp trailing edge. This augments aerodynamic forces by entraining and deflecting the aerofoil flow-field pneumatically, rather than solely deflecting a mechanical surface. The aerodynamic concept is known as circulation control.

As it is applied to a typical fixed aircraft, the concept employs engine bleed air blown tangentially over a curved trailing edge to amplify the aerofoil circulation and thus its high lift capability. The tangential jet sheet exits over the curved trailing edge of the surface replacing the mechanical flap; this curvature can turn through a full 180°. The jet will remain attached to the curved surface because of a balance between the sub-ambient pressure in the jet sheet and the centrifugal force around the curvature of the surface, see Fig. 1. At very low blowing levels, the jet entrains the boundary layer to prevent aft flow separation, and thus it is very effective for boundary layer control (BLC). As the jet continues to turn, a rise in static pressure plus viscous shear stress and centrifugal force combine to separate the jet sheet, and a new stagnation point and streamline are formed on the lower surface. The large flow entrainment rate of the jet and deflection of the stagnation streamline produce a pneumatic camber similar to a mechanical high lift system, and thus pneumatic control of the aerofoil's circulation and lift is achieved.

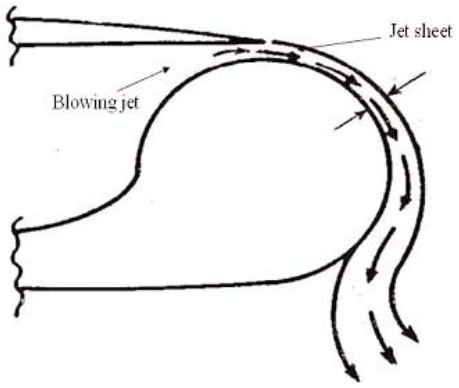


Figure 1. Circulation control[1].

Although circulation control is a very effective for boundary-layer control (BLC), the interest in this technology comes from its ability to further augment the circulation and lift with flow turning and control of leading edge streamlines. Lanchester, Kutta, and Joukowski laid the foundation for a quantitative theory relating the lift to an infinite wing through the integration of the velocity field along a streamline[2].

The circulation control (CC) concept is actually based on the Coanda effect, named after the Romanian inventor Henri Coanda who claimed to have discovered it in Paris prior 1935[3]. In 1967, Kind and Maull[4] began to study the boundary layer around a Coanda aerofoil. Their results demonstrated that the jet issuing from the slot delayed the separation of the upper surface boundary layer and caused the flow about the aerofoil to be asymmetric. Thus, the circulation around the aerofoil was controlled by the strength of the jet. The aerodynamic characteristics of circulation control wings (CCW) have been experimentally and numerically studied for more than 65 years.[5,6,7]. Many of these studies have concentrated on trailing-edge shape, slot height and blowing rates. Results of these studies highlighted geometric features that affect aerofoil performance such as the ratio of trailing-edge radius to chord (r/c), slot height to chord (h/c), slot height to trailing-edge radius (h/r), and Coanda surface shape.

The study of CC-supercritical aerofoil combination was first conducted by Englar in 1981[8]. The results of subsonic two-dimensional wind-tunnel investigations indicated that a small trailing-edge size can be applied to a supercritical aerofoil without degrading CC performance. The base drag was minimised by the small trailing-edge radius, so that un-blown C_d was essentially the same as that of the baseline supercritical section. It was also shown that the drag could be further reduced to less than that of the baseline aerofoil by minimal blowing. He also reviewed the effects of high-velocity ratios U_J/U_∞ by using a smaller trailing-edge radius[9]. The lift coefficient as a function of the jet velocity ratio has also been examined by other researchers[10]. High lift augmentation ratios (i.e. lift due to blowing/jet thrust) of up to 14 were achieved at the optimum blowing conditions. Previous studies on CC aerodynamics have shown various benefits on the lift augmentation for short take off and landing (STOL) flights[11]. Spaid and Keener[12] conducted an experimental investigation with wind-tunnel measurements of boundary layer and wake velocity profiles of a swept circulation-control wing. For the selected jet-blowing rates an abrupt transition from incipient separation to attached flow occurred in the boundary-layer upstream of the slot. The results showed that the flow in the vicinity of the jet-exit (near wake) was highly three-dimensional, and large outboard flow was observed at the centre of the wake. Conventional CC pneumatic systems often involve arrays of actuators installed inside the wing section[13], which can increase the weight of the vehicle. The volume requirement penalties related to the internal air delivery systems can often be problematic for wing assembly. Therefore, there is the need to simplify and to reduce the weight of these pneumatic systems without sacrificing performance.

For two-dimensional CC studies, the thrust can be described at the jet exit of the aerofoil by the blowing momentum coefficient C_μ. The blowing momentum coefficient was introduced in 1948[14] to make possible the interpretation of experimental results with blowing and it is defined as

$$C_\mu = \frac{Thrust}{qS} = \frac{\dot{m}(U_J)}{q(c)(b)} \quad \ldots (1)$$

where

$$\dot{m} = \rho_J U_J A_J \quad \ldots (2)$$

and

$$U_J = \sqrt{\frac{P_t - p_s}{0{\cdot}5\rho_J}} \quad \ldots (3)$$

https://doi.org/10.1017/S0001924000002773 Published online by Cambridge University Press

The profile drag of the Coanda aerofoil with the application of blowing must be corrected by adding the momentum that was added by the blowing system. This is done by assuming a frictionless condition. The jet momentum is converted into a force which is quantified by the mass flow rate times the freestream velocity[15]. The corrected profile drag coefficient is given by Equation (4).

$$C_{dpc} = C_{dp} + C_{\mu}\frac{U_{\infty}}{U_J} \quad \ldots (4)$$

Therefore, the profile drag coefficient for the Coanda aerofoil with and without blowing can be compared. However, to make direct comparison of the Coanda aerofoil with steady blowing at different blowing momentum coefficients, it is necessary to define an equivalent lift-to-drag ratio. This is because the system efficiency should contain the effects of the energy input that is required to achieve the aerofoil performance. It would also avoid the infinite efficiency that occurs when the drag goes to zero due to high blowing momentum[16]. The correction is made through an equivalent 'kinetic energy' drag coefficient that is related to the power. For a crude estimate of fluid power, it is assumed that the jet is taken from a large reservoir. The total power requirement is at least equal to the power required to supply the jet velocity head plus the power lost at the intake as the fluid is drawn into the large reservoir. This equivalent drag can be described as

$$D_{EQUIV} = D_{dp} + D_{Power} + D_{RAM} \quad \ldots (5)$$

The equivalent drag coefficient and performance are calculated from Equations (6) and (7) respectively. The non-dimensional form of the fluid power can be expressed in terms of C_{μ}

$$C_{d_{EQUIV}} = C_{dp} + C_{\mu}\frac{U_J}{2U_{\infty}} + C_{\mu}\frac{U_{\infty}}{U_J} \quad \ldots (6)$$

$$\frac{L}{D_{EQUIV}} = \frac{C_l}{C_{d_{EQUIV}}} \quad \ldots (7)$$

The objectives of the present investigation are to examine the application of a uniform tangential steady jet across the span of a Coanda aerofoil in both the boundary-layer control (BLC) and circulation control (CC) regimes, and its effects to boundary-layer properties and wake characteristics. Through the study of the aerodynamic forces and moments of the Coanda aerofoil, the authors aim to present the power requirement in order to maximise aerofoil performance.

2.0 EXPERIMENTAL SETUP

The model used is a 17-percent thick circulation control/supercritical aerofoil combination which has a Coanda trailing edge. This aerofoil has been proven to be suitable for low-speed general aviation applications, such as propeller driven light aircrafts[17,18]. The geometry is based on the model investigated by Englar in 1981[8]. The aerofoil consists of a solid aluminum section, with the rear inside portion removed to create the internal plenum, and a trailing-edge section which covers the plenum to maintain the supercritical geometry. The geometry is shown in Fig. 2.

The span of the base section is 732mm. Several designs of the internal plenum were considered and tests were carried out to investigate the level of uniformity of blowing jet across the trailing edge of the Coanda aerofoil[19]. The plenum of the chosen design is fitted with a honeycomb and two identical triangular sections. The side of each triangular section facing the Coanda trailing edge is a mesh of finely drilled holes to produce numerous air jets directed towards the honeycomb

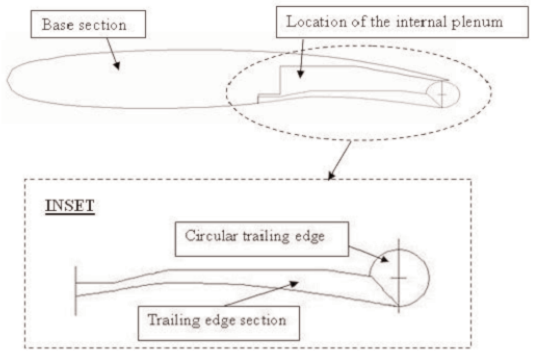


Figure 2. Base- and trailing-edge sections geometry.

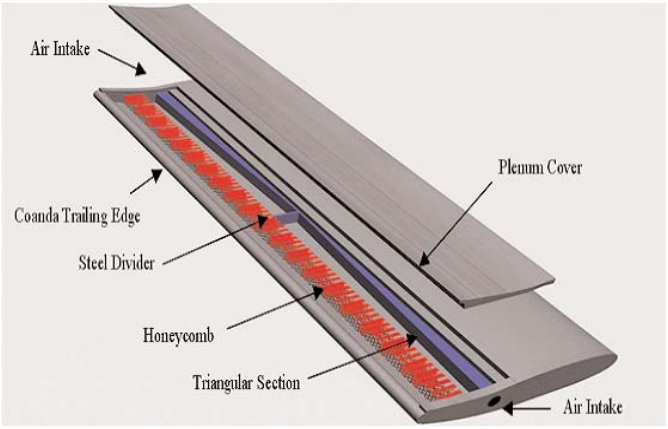


Figure 3. Layout of the internal plenum.

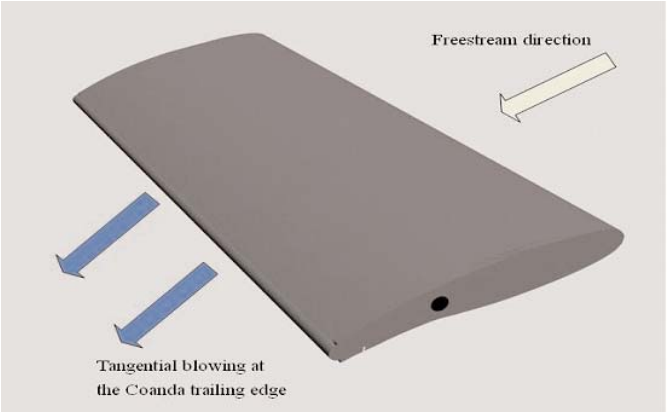


Figure 4. External view of the Coanda aerofoil.

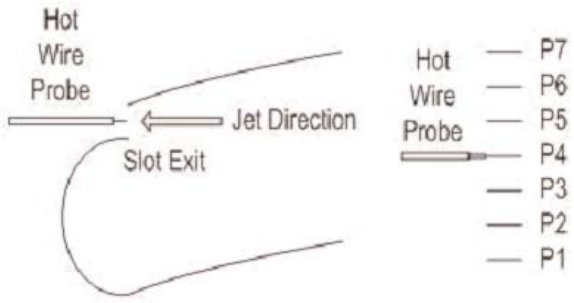


Figure 5. Locations of measurements along the span of the aerofoil at the slot exit.

https://doi.org/10.1017/S0001924000002773 Published online by Cambridge University Press

Table 1
Overall dimensions of the Coanda aerofoil.

Trailing-edge Radius	Slot Height	Chord Length
9·5mm	1 ± 0·25mm	279mm

section. Each mesh has 100 holes of 0·5mm diameter evenly distributed in a matrix of 5 × 20 The area of each mesh is (357 × 17) mm^2. In the middle of the plenum, (upstream of the honeycomb), a thin steel divider is used to separate the volume in half. The complete design is shown in Fig. 3. There are two air inlets on either side of the base section, so that the plenum can be filled with compressed air. The compressed air is controlled by a pressure regulator. It has an operating range from 0·4 to 10bar with a built-in pressure gauge which has a resolution of 0·25bar. A complete external view of the aerofoil is depicted in Fig. 4. The dimensions of the Coanda aerofoil are shown in Table 1.

For the measurement of the steady jet velocity and the turbulence characteristics, a single-component hotwire anemometer (DISA 55M01) was used. The constant overheat ratio was set at 0·8[20]. The single-component hotwire sensor was aligned parallel to the span and was positioned at the slot exit (x/c = 0·98). The locations of measurements are shown in Fig. 5. Position 4 is located in the mid span of the aerofoil. The distance between each position is equal to 87·5mm. The inlet pressure was regulated at 0·5 bar, 1·0 bar, 1·5 bar, 2·0 bar and 2·5 bar. The velocity signals from the signal processor were collected through an A/D converter and were saved onto the data-processing PC. The accuracy for the mean velocity and turbulent measurements is 2% and 2·5% respectively.

A subsonic, open circuit, suction tunnel with a 0·92m (width) × 0·92 m (height) × 3·64 m (length) test section was used. The investigation was conducted using a two-dimensional aerofoil. False floor and ceiling were installed in the wind-tunnel. The turbulent intensity is 0·07%. The experiments were performed at freestream velocity U_∞ of 14ms^{-1} and Reynolds number of 2·67 × 10^5. (based on the aerofoil chord length). The freestream flow in the test-section is laminar at this low Reynolds number. This avoids excessive turbulent mixing between the blowing jet and the freestream flow at the trailing edge in both BLC and CC regimes. The low Reynolds number offers high blowing momentum around the Coanda trailing edge without excessive power input, thus the required blowing momentum is reduced in the CC flow control regime.



Figure 6. Custom-made boundary-layer survey rig and aerofoil arrangement.

Boundary-layer properties were measured with a single-component hotwire anemometer (DISA 55M01) along the mid span of the suction surface at x/c equal to 0·25, 0·50, 0·75 and 0·95 (indicated as stations 1 to 4 respectively), and around the circular trailing edge. The data were taken for two seconds at a sampling rate of 10kHz. Velocity profiles at different angular positions were acquired by moving the custom-made boundary-layer survey rig around the Coanda trailing edge. The experimental layout and boundary-layer survey rig are shown in Fig. 6. The initial position of the hotwire sensor was set at 1mm above the surface. The data were averaged from three data logs.

To avoid any misleading results of the drag from the force balance due to the addition of momentum from the tangential blowing, the profile drag was measured using the wake-traverse method proposed by Jones[21]. A survey plane was selected at 0·43c away from the trailing edge of the aerofoil and velocity measurements were taken at the mid span of aerofoil. The single-component hotwire anemometry (DISA 55M01) was employed to determine the mean velocity deficit in the wake. In order to record the unsteadiness inside the wake, a high sampling rate of 10kHz was used.

The lift forces and pitching moments were measured at different blowing momentum coefficients with a 3-component external strain gauge balance. A 12-bit data acquisition system with a moderate sampling rate of 512Hz was used, and the time-averaged (mean) lift forces and pitching moments were measured. The calibration of the load cells indicated that the lift force and pitching moment coefficient measurement had an error of approximately ±0·03%. Aerodynamic forces were normalised by the freestream dynamic pressure q and aerofoil area S. The aerofoil chord was used as the reference length for the normalisation of the pitching moments. The presented data are corrected for the solid and wake blockage.

3.0 RESULTS AND DISCUSSIONS

3.1 Calibration of steady blowing jet

The steady jet velocity at different positions along the slot exit was measured, and the degree of jet uniformity was determined. The time-averaged (mean) blowing momentum coefficient was calculated from

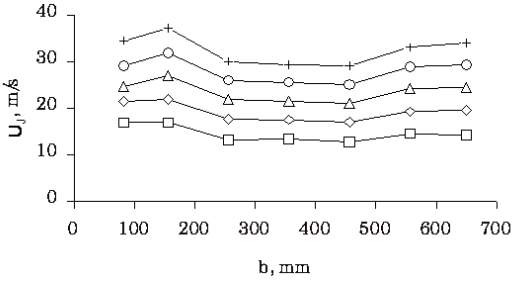


Figure 7. Steady jet velocity measurement at the slot exit; □, P_t = 0·5 bar; ◇, P_t = 1·0 bar; Δ, P_t = 1·5 bar; ○, P_t = 2 bar; +, P_t = 2·5 bar.

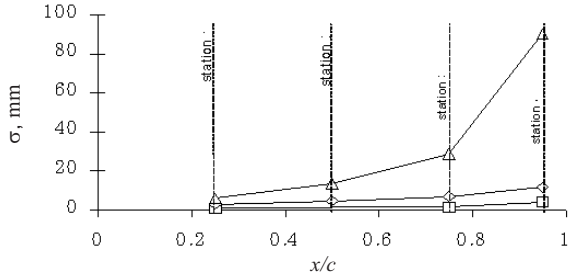


Figure 8. Boundary-layer thickness along the mid span of the aerofoil at C_μ = 0·013 (within BLC regime); □, 0° AoA; ◇, 6° AoA; Δ, 13° AoA.

https://doi.org/10.1017/S0001924000002773 Published online by Cambridge University Press

Table 2
Time-averaged (mean) blowing momentum coefficients at different inlet pressures

P_j, bar	U_∞,ms^{-1}	Mean C_μ	Mean U_j, ms^{-1}	Mean RTI, %	Mass Flow Rate, Kg/s
0·5	14	0·008	14·63	0·62	0·013
1·0	14	0·013	19·28	0·63	0·017
1·5	14	0·020	23·61	0·65	0·021
2·0	14	0·028	28·10	0·66	0·025
2·5	14	0·038	32·57	0·67	0·028

Equation (1). The latter serves as an indication of the lift augmentation within the force measurement. An accurate steady jet velocity measurement at the mid-span aids the calculation of the equivalent drag of the Coanda aerofoil.

Figure 7 shows the steady jet velocity at different positions along the span of the circular trailing edge. Since the mass flow rate is directly proportional to the slot height for one-dimensional flow (i.e. at a singular point along the span), the steady jet uniformity at different positions along the span of the aerofoil is governed by the slot height. It can be seen that the jet velocity near both edges is generally higher than that at the mid-span. Screws are installed on both sides of the aerofoil to adjust correctly the slot height. Any slight misalignment on the screw fastenings will cause small difference in the slot height, which will cause the variations observed in Fig. 7. The slot height at the mid span is slightly higher than the sides. On the other hand, the velocity difference on the left and right sides of the slot is due to the small variation of tightness of the screws attaching the trailing-edge and base sections together. As the jet pressure increases from 0·5 to 2·5 bar, the variation in the jet velocity along the span increases from 20% to 26%. The accuracy of the measurements discussed in Section 2 'Experimental Setup' has taken into consideration the discrepancies in jet velocity distribution across the span. These discrepancies have a minor effect on the present measurements as all data collected have been time-averaged. Table 2 shows the summary of the time-averaged (mean) blowing momentum coefficients for different inlet pressures. With increasing pressure from 0·5 to 2·5bar, the mean blowing momentum coefficient C_μ is approximately a second order polynomial function to the inlet pressure. The relative turbulent intensity (RTI) increases from 0·62% to 0·67%; this indicates that the steady jet has a low turbulence along the span of aerofoil for all cases considered.

3.2 Boundary-layer measurements

Figure 8 shows the boundary-layer thickness along the mid span of the aerofoil in BLC regime. At zero angle-of-attack, a relatively thin boundary-layer exists over the suction surface of the aerofoil. The boundary-layer thickness is increased from 1·01mm to 4·04mm between stations 1 and 4. The boundary-layer is thicker compared with the no-blowing case[19]. This is due to the turbulent region near the trailing edge induced by the steady jet. At 6o angle-of-attack, the boundary-layer thickness increases from 3·02mm (at x/c = 0·25) to 11·65mm (at x/c = 0·95). This proves that the circulation around the aerofoil has changed slightly within the boundary-control regime.

At 13o angle-of-attack, the boundary-layer thickness increases from 6·02mm (at x/c = 0·25) to 90·18mm (at x/c = 0·95), and it is larger than that of the no-blowing case[19]. It also increases abruptly at station 4 due to the separated flow over the suction surface, and a trailing edge stalling characteristic is observed. It was not possible to measure the boundary-layer thickness at 17° angle-of-attack due to the unstable platform generated with the strong momentum jet at the trailing edge.

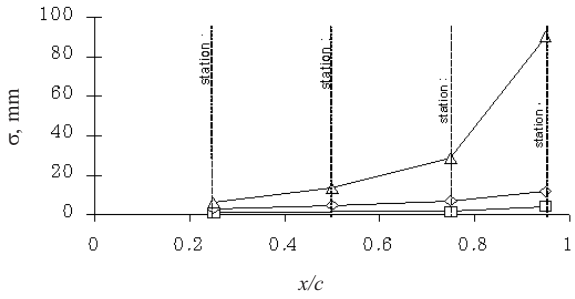


Figure 9. Boundary-layer thickness along the mid span of the aerofoil at C_μ = 0·038; □, 0° AoA; ◇, 6° AoA; Δ, 13° AoA.

Table 3 shows the boundary-layer properties around the circular trailing edge when C_μ is equal to 0·013. The shape factor is less than 1·40 for angular position θ_A between 20° and 100° without the presence of freestream flow. This shows that the steady jet remains attached to the circular trailing edge from the slot (i.e. θ_A = 0) to approximately 105° to 120° and no subsequent reattachment is detected.

At 0° angle-of-attack, the jet separation angle θ_s is about 45° to 55° since the shape factor increases from 1·30 to 2·21 and no subsequent flow reattachment is detected. It is noted that θ_s is affected by the freestream flow velocity. The large velocity differential between the jet and the freestream flow would normally cause the loss of the angular momentum of jet to take place nearer the slot. However, the jet also encounters a freestream flow coming from the bottom side of the aerofoil and this triggers the flow to separate earlier than the one without the freestream. At 6° angle-of-attack, θ_s is about 45° to 55° since the shape factor increases from 1·33 to 1·85. It is also noted that the shape factor is decreased from 1·56 to 1·35 at θ_A between 65° and 75°. This indicates the formation of the single separation bubble within the small angular displacement. The flow reattaches to the circular trailing edge and it is more turbulent. At 13° angle-of-attack, θ_s is about 45° since the shape factor increases to 1·56. The shape factor decreases from 1·57 to 1·41 at θ_A between 65° and 75°. This again indicates a possible flow reattachment after the formation of the separation bubble. At 17° angle-of-attack, θ_s is less than 20° around the circular trailing edge since the shape factor is 1·41. The flow reattaches to the surface at θ_A between 20° and 30°, as the shape factor decreases from 1·41 to 1·17. The flow separates again at θ_A between 30° and 45°. Therefore, the change of angle-of-attack promotes flow separation around the circular trailing edge, which reattaches to the surface after the formation of a separation bubble.

Figure 9 shows the boundary-layer thickness along the mid span of the aerofoil in CC regime. It can be seen that a relatively thin boundary-layer exists at zero angle-of-attack. The boundary-layer thickness increases from 0·96mm to 3·02mm between stations 1 and 4. The boundary-layer is thinner than that measured for C_μ = 0·013 case (see Fig. 8). This suggests a change of the stagnation point around the leading edge due to the strong angular momentum at the trailing edge, which causes the alternation of circulation around the aerofoil. At 6° angle-of-attack, the boundary-layer thickness increases from 3·65mm (station 1) to 9·65mm (station 4). Again, it is less than that measured for C_μ = 0·013 case. Its reduction is due to the higher velocity flow field which circulates around the aerofoil in the circulation control regime. At 13° angle-of-attack, the boundary-layer thickness increases from 8·27mm at the leading edge (station 1) to 90·18mm (station 4), and it is similar to that measured when C_μ = 0·013. It is conjectured that the increase of blowing momentum coefficient does not affect the flow momentum within the boundary-layer near the slot exit. The boundary-layer thickness increases abruptly at station 4 due to the separated flow over the suction surface. Therefore, a trailing-edge stalling characteristic is also observed within the circulation control regime.

https://doi.org/10.1017/S0001924000002773 Published online by Cambridge University Press

Table 3
Boundary-layer properties around the circular trailing edge of the Coanda aerofoil (C_μ = 0·013)

U_∞ = 0ms^{-1}

θ_A, deg	55	65	75	90	100	120	130
δ*	0·011	0·037	0·055	0·121	0·188	0·289	1·313
θ	0·001	0·031	0·046	0·092	0·144	0·190	0·648
ε	0·018	0·057	0·084	0·165	0·259	0·326	1·036
H_1	1·13	1·19	1·20	1·32	1·30	1·52	2·03

U_∞ = 14ms^{-1} 0° AoA

θA, deg	20	30	45	55	65	75	90
δ*	–	–	0·145	1·053	2·299	2·611	–
θ	–	–	0·112	0·477	0·920	1·114	–
ε	–	–	0·199	0·743	1·387	1·677	–
H_1	–	–	1·30	2·21	2·50	2·34	–

U_∞ = 14ms^{-1} 6° AoA

θA, deg	20	30	45	55	65	75	–
δ*	–	–	0·043	0·311	0·192	0·136	–
θ	–	–	0·032	0·168	0·123	0·100	–
ε	–	–	0·057	0·275	0·206	0·177	–
H_1	–	–	1·33	1·85	1·56	1·35	–

U_∞ = 14ms^{-1} 13° AoA

θA, deg	20	45	55	65	75	90	120
δ*	–	0·1811	0·520	0·724	0·550	41·048	10·735
θ	–	0·1164	0·306	0·463	0·391	17.838	3·268
ε	–	0·1953	0·508	0·788	0·682	26.297	4·613
H_1	–	1·56	1·70	1·57	1·41	2·30	3·28

U_∞ = 14ms^{-1} 17° AoA

θA, deg	20	30	45	55	65	75	90
δ*	0·088	0·051	0·226	0·359	0·312	0·501	–
θ	0·062	0·044	0·119	0·181	0·169	0·314	–
ε	0·107	0·081	0·190	0·287	0·270	0·526	–
H_1	1·41	1·17	1·90	1·99	1·85	1·60	–

Table 4
Boundary-layer properties around the circular trailing edge of the Coanda aerofoil at C_μ = 0·0380

U_∞ = 0ms^{-1}

θ_A, deg	55	65	75	90	100	120	130
δ*	0·010	0·012	0·028	0·050	0·068	0·093	0·643
θ	0·008	0·011	0·025	0·043	0·060	0·070	0·391
ε	0·014	0·021	0·047	0·080	0·112	0·128	0·650
H_1	1·26	1·09	1·12	1·17	1·14	1·32	1·65

U_∞ = 14ms^{-1} 0° AoA

θ_A, deg	20	30	45	55	65	75	90
δ*	–	–	0·002	0·074	0·251	0·345	1·618
θ			0·002	0·057	0·169	0·222	0·704
ε	–		0·004	0·102	0·290	0·376	1·090
H_1	–	–	1·00	1·29	1·48	1·55	2·30

U_∞ = 14ms^{-1} 6° AoA

θ_A, deg	20	30	45	55	65	75	90
δ*	–	–	0·005	0·082	0·059	0·112	–
θ–	–	0·004	0·054	0·048	0·086	–	–
ε	–	0·008	0·092	0·086	0·154	–	–
H_1	–	–	1·03	1·53	1·24	1·30	–

U_∞ = 14ms^{-1} 13° AoA

θ_A, deg	20	30	45	55	65	75	90
δ*	–	–	0·014	0·170	0·245	0·232	–
θ–	–	0·125	0·103	0·129	0·149	–	–
ε–	–	0·024	0·171	0·207	0·252	–	–
H_1	–	0·11	1·65	1·89	1·55	–	–

U_∞ = 14ms^{-1} 17° AoA

θ_A, deg	20	30	45	55	65	75	90
δ*	–	–	0·101	0·134	0·185	0·228	0·596
θ–	–		0·061	0·078	0·103	0·143	0·396
ε–	–		0·100	0·128	0·167	0·243	0·673
H_1	–	–	1·66	1·72	1·80	1·59	1·51

Table 4 shows the boundary-layer properties around the circular trailing edge at C_μ equal to 0·038. The shape factor is less than 1·40 for angular position θ_A between 20° to 120° without the presence of the freestream flow (i.e. U_∞ = 0ms^{-1}). This shows that the flow remains attached to the circular trailing edge from the slot (i.e. θ_A = 0) until 125° to 130°. No subsequent reattachment is detected. The result indicates that the flow stays attached to the surface for a larger angular position θA with increasing blowing momentum coefficient.

At 0° angle-of-attack, the angular separation angle θs is approximately between 65° to 75° since the shape factor increases from 1·48 to 1·55 and no subsequent flow reattachment is detected. θs has increased compared with the one obtained at C_μ equal to 0·013. This is because the jet velocity is larger and this produces higher angular momentum at the slot. At 6° angle-of-attack, θs is about 45° to 55° since the shape factor increases from 1·03 to 1·53. The shape factor is decreased from 1·53 to 1·24 at θ_A between 55° to 65°. This indicates the formation of the single separation bubble within the small angular displacement. The flow reattaches to the circular trailing edge and it is more turbulent. The flow remains attached to the circular trailing edge for θ_A over 75°. It is believed that the flow separates at θ_A equal to 90°. Therefore, the increase of the jet momentum causes the formation of a smaller separation bubble and the flow reattaches to the surface for a larger angular displacement.

At 13° angle-of-attack, θ_s is about 45° to 55° since the shape factor increases from about 0·11 to 1·65. As the shape factor is larger than 1·40 for θ_A = 55°, the flow remains separated. This is probably due to the increase of flow turbulence at the flow separation location, which is non-favorable to the formation of separation bubble. At 17° angle-of-attack, θ_s is less than 45°, as the shape factor is 1·66. No flow reattachment was detected. The increase of jet momentum (i.e. the change from BLC to CC regime) delays the flow separation location; however, the formation of the separation bubble is not permitted within the circulation control regime at high angles-of-attack. This is probably due to the increase of turbulence intensity of the steady jet ahead of the location of separation, due to the mixing of the flow.

4.0 WAKE MEASUREMENTS

Fig. 10 shows the wake profile behind the trailing edge of the Coanda aerofoil with steady jet at C_μ equal to 0·007 (within the BLC regime). At zero angle-of-attack, the maximum velocity deficit is 17% at *y*/*w* equal to 0·46, which is identical to the no-blowing case[19]. The additional mass flow at the trailing edge diffuses rapidly into the surroundings and it does not penetrate into the wake of the aerofoil sufficiently. As a result, the wake width is expected to vary. As the angle-of-attack increases to 6°, the maximum velocity deficit is approximately 43% at y/w equal to 0·5. The maximum velocity deficit has increased significantly from 17% to 43%.

https://doi.org/10.1017/S0001924000002773 Published online by Cambridge University Press

At 12° angle-of-attack, the maximum velocity deficit is 67% at y/w equal to 0·61· The location of the maximum velocity deficit is larger than the half of the wake width. This indicates the lower portion of the wake (i.e. probably generated from the lower surface of the aerofoil) is entrained by the steady jet, and the jet does not generate a noticeable effect to aid the delay of the flow separation on the upper surface of the aerofoil. At 13° angle-of-attack, the maximum velocity deficit is about 74% at *y/w* equal to 0·63, and its location is similar to the no-blowing case[19]. It increases slightly with the application of the steady jet which further suggests that the jet diffuses into the surroundings. The rate of diffusion becomes larger as the angle-of-attack increases, since the surrounding fluid from the separation has less momentum. Further increasing the aerofoil incidence to 14°, the maximum velocity deficit is even higher, and its width decreases slightly. Beyond the stalling incidence (at 20° angle-of-attack), a similar effect of reduced maximum velocity deficit is observed. Therefore, it can be concluded that the wake is entrained by means of reducing the maximum velocity deficit region; however, the width of the wake is expected to increase due to the diffusion of jet momentum across the freestream.

Figure 11 shows the wake profile behind the trailing edge of the Coanda aerofoil with steady jet at C_μ equal to 0·013 (within BLC regime). At zero angle-of-attack, the maximum velocity deficit is about 24% at *y/w* equal to 0·50, which is increased significantly compared with the case when C_μ = 0·007. The additional jet momentum diffuses more rapidly into the surroundings, however, this is not associated with the flow separation angle around the circular trailing edge. It depends only on the jet velocity leaving the Coanda surface. At 6° angle-of-attack, the maximum velocity deficit is about 51% when *y/w* = 0·45. This indicates a larger increase of the maximum velocity deficit compared to both the no-blowing case and the case when C_μ equal to 0·007. The rate of jet diffusion is increased and this would effectively reduce the wake width. Conversely, the wake width is increased with tangential blowing at C_μ = 0·013 and at high angles-of-attack. From 12° to 14° angles-of-attack, similar effects of additional jet momentum are observed; the maximum velocity deficit is increased, and the increase of diffusion rate of the jet reduces the wake width. However, the maximum velocity deficit is 75% which is similar to the case when C_μ equal to 0·007. This shows that the diffusion rate is affected by the angle-of-attack, especially for larger than stalling incidence settings.

Figure 12 shows the wake profile behind the trailing edge when C_μ = 0·038 (CC regime). At zero angle-of-attack, the maximum velocity deficit is 17% at *y/w* = 0·46; the diffusion rate of the jet momentum is reduced significantly, and the centre of the wake is greatly energised. Therefore, both the relative turbulence intensity and the wake width are expected to reduce significantly. A similar observation is found at 6° angle-of-attack, where the maximum velocity deficit is about 34% at *y/w* = 0·5. The diffusion rate of the steady jet is reduced when a high blowing momentum coefficient is used. It can be described as a pneumatic camber similar to a mechanical high lift system at which the steady jet leaves the circular trailing edge; the divergence of the shear layers is reduced. It is also thought that the jet entrainment becomes less apparent as the displacement from the trailing edge increases. Above 12° angle-of-attack, the wake width is expected to reduce significantly for the conservation of mass flow. Therefore, the additional mass flow inside the wake becomes a tool for controlling the wake profile and the wake width, and it reduces the relative turbulence intensity inside the wake at high blowing momentum coefficients.

Figure 13 shows the maximum relative turbulent intensity (RTI) within the wake profiles at different blowing configurations. At zero angle-of-attack, the maximum RTI is reduced with increasing C_μ. This is the primary effect of the entrainment of additional mass flow inside the wake. Also, the maximum RTI depends on the jet pressure when leaving the circular trailing edge, and that is affected by the pressure differential between the jet and the ambient conditions

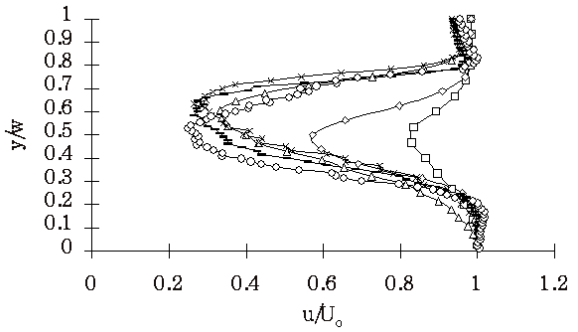


Figure 10. Wake profiles behind the trailing edge of the Coanda aerofoil with steady jet at C_μ = 0·007; □, 0° AoA; ◇, 6° AoA; Δ, 12° AoA; x, 13° AoA; -, 14° AoA; ○, 20° AoA.

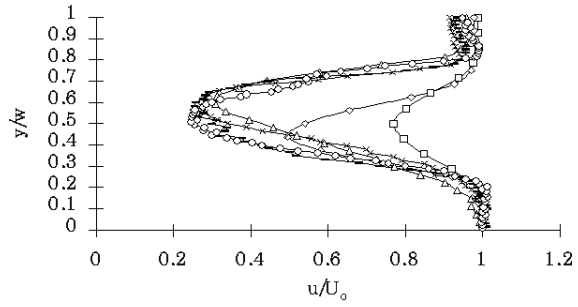


Figure 11. Wake profiles behind the trailing edge of the Coanda aerofoil with steady jet at C_μ = 0·013; □, 0° AoA; ◇, 6° AoA; Δ, 12° AoA; *x*, 13° AoA; -, 14° AoA; ○, 20° AoA.

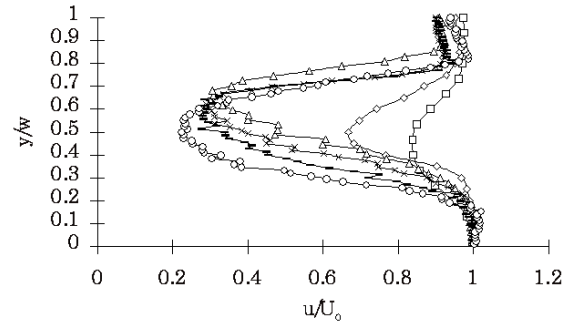


Figure 12. Wake profiles behind the trailing edge of the Coanda aerofoil with steady jet at C_μ = 0·038; □, 0° AoA; ◇, 6°o AoA; Δ, 12° AoA; *x*, 13° AoA; -, 14° AoA; ○, 20° AoA.

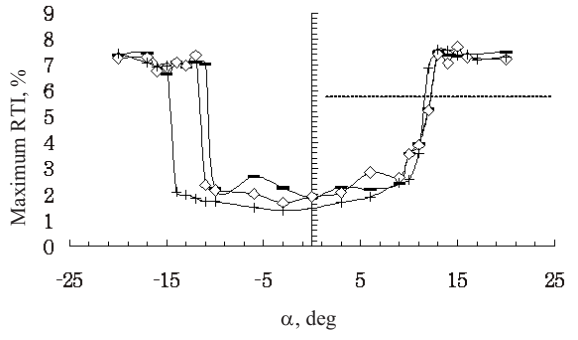


Figure 13. Maximum RTI for Coanda aerofoil with steady jet; -, C_μ = 0; ◇, C_μ = 0·013; +, C_μ = 0·038.

https://doi.org/10.1017/S0001924000002773 Published online by Cambridge University Press

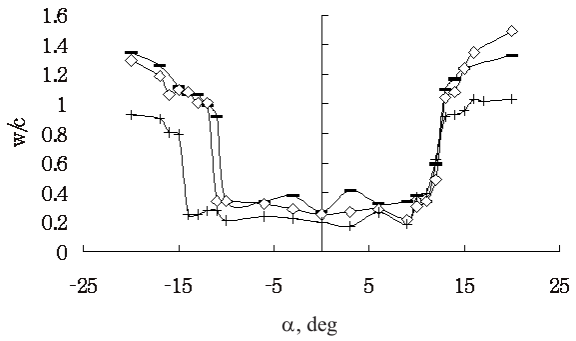


Figure. 14 Comparison of wake-width to chord ratios; -, C_μ = 0; ◇, C_μ = 0·013; +, C_μ = 0·038.

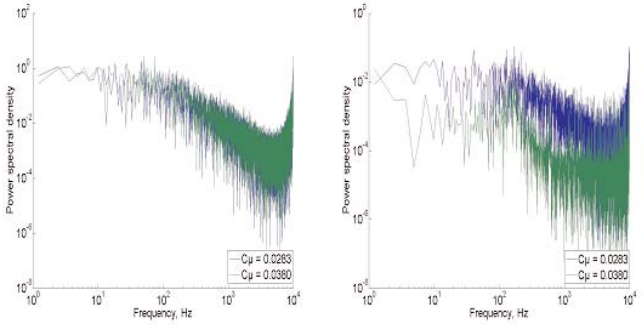


Figure 15. Spectral analysis for Coanda aerofoil with steady jet (α = 11 Figure AoA); a) *y/w* = 0·5; b) *y/w* = 0·9.

inside the test section. With increasing angle-of-attack, the centrifugal force is altered around the circular trailing edge due to the change in local pressure. Therefore, the jet pressure at which leaving the circular trailing edge is changed, and this alters the maximum RTI inside the wake. On the other hand, the maximum RTI does not indicate the stalling characteristics as compared with the aerofoil with hinged flap, see Ref. 19. It shows that the maximum RTI is remains almost constant within the different flow control regimes. The change of pneumatic camber by the jet has demonstrated that the momentum is insensitive to relative turbulent intensity inside the wake at high incidences. It shows a controversy compared to the aerofoil with hinged flap, which has an identical geometry (except the sharp trailing edge) to the Coanda aerofoil, that the stalling characteristics can be described with increasing maximum RTI[19].

Fig. 14 shows the wake-width to chord (*w/c*) ratio for the Coanda aerofoil for both BLC and CC regimes. The variation of w/c is particularly sensitive between 3° and 9° angles-of-attack. It is believed that w/c is associated to boundary-layer and circulation control regimes. When C_μ = 0·038, it shows a significant reduction of the wake width. This is due to the location of jet separation and the turbulent mixing between the induced shear layer of the jet and the wake. However, it was not possible to confirm such characteristic with a higher blowing momentum coefficient in the present investigation. On the other hand, *w/c* remains almost unchanged between 11° and 13° angle-of-attack for both BLC and CC regimes. This indicates the characteristics of the wake width are insensitive to the regimes in those incidences for the present aerofoil geometry. For above 15° angles-of-attack, w/c is reduced by about 30% when C_μ = 0·0380· This indicates that the steady jet separates from the circular trailing edge more easily at high angles-of-attack. This mainly depends on the upstream flow conditions. Therefore, the jet diffuses into the wake region, and this reduces the wake width. The current results suggest that the wake width is greatly affected by the location of jet separation, and the strength of the steady jet which is associated with the relative turbulent intensity. For a high momentum jet, the wake width is reduced at a fixed location downstream compared with the low momentum jet. Therefore, it seems beneficial to use a high momentum jet rather than a low momentum jet within the CC regime at high aerofoil incidences as the wake width is reduced.

In Ref. 19, the spectral analysis at the centre of the wake (*y/w* = 0·5) of the Coanda aerofoil at 12° angle-of-attack and C_μ = 0·007 shows that the PSD level is the highest at 9·76Hz. A second harmonic of 19·52Hz is also observed. The PSD levels are increased compared to those for the no-blowing case. This indicates that the wake behind the aerofoil is more turbulent, and it is mainly responsive to the low frequencies. It also means that the wake is dominated by the effect of the steady jet in the low frequency range. Furthermore, the PSD level is nearly identical to the no-blowing case for above 300Hz. Therefore, the additional mass flow does not create high frequency turbulence inside the wake, and the energy loss of the steady jet is mainly due to the viscosity instead of the momentum diffusion at the centre of the wake. Whereas at the edge of the wake (*y/w* = 0·9), for the same angle-of-attack, the diffusion of the steady jet is more pronounced. The PSD level increases when the steady jet is applied, but the frequency response remains unchanged for both the no-blowing case and the case when C_μ = 0·007.

When C_μ is increased from 0·007 to 0·013, the PSD peaks are found between 7·34Hz and 43·95Hz. Peaks are also found between 7·34Hz and 21·97Hz when C_μ = 0·02. Therefore, the flow fluctuates at lower frequency when a higher C_μ is used. In addition, the flow fluctuation is increased due to the higher PSD level observed in Ref. 19. On the other hand, the momentum diffusion of the jet at the edge of wake is less vigorous at high blowing momentum coefficients. This means the addition of jet momentum suppresses the PSD levels, and it improves the stability at the edge of the wake.

Figure 15(a) and Fig. 15(b) show the power spectral density at the centre, and the edge of the wake respectively for 11° angle-of-attack. Fig. 15(a) indicates that distinct peaks are located at 50·05Hz and 74·46Hz when C_μ = 0·038, whereas the distinct peaks are located at 18·31Hz, 28·08Hz and 46·39Hz when C_μ = 0·0283. This shows that a higher frequency response is obtained when a higher C_μ is used. Also, the PSD levels corresponding to the peaks are higher at C_μ = 0·038.

The reduction of the PSD level for the whole range of frequencies is observed in Fig. 15(b) when C_μ = 0·038. This suggests the reduction of flow fluctuation at the edge of the wake with the use of high momentum jet, which also increases the flow stability. It is evident that the stability of the wake edge is dominated by the strength of the steady jet.

5.0 FORCE MEASUREMENTS

In Ref. 19, the lift coefficient at zero angle-of-attack is increased from 0·38 to 0·77 with increasing blowing momentum coefficient from 0 to 0·038. This increase of lift coefficient is approximately 100%, and the effect of attached flow at the circular trailing edge is demonstrated. When the steady jet is applied at C_μ is equal to 0·013 (i.e. within BLC regime), the maximum lift coefficient is found at 14o angle-of-attack, which is similar to the value in the no-blowing case. The angle-of-attack for the maximum lift coefficient is progressively reduced from 14° to 11° when C_μ is increased from 0·013 to 0·038 (i.e. BLC to CC regime). This lift characteristic shows a similar effect to the positive flap deployment. The circulation of the aerofoil is altered with the application of high momentum steady jet. Ref. 19 shows a slow stall which is typical of a thick aerofoil, where the separation advances slowly towards the leading edge as angle-of-attack increases. The initial observation by Wong[19] has proved that the use of steady tangential blowing to increase lift is effective; this

https://doi.org/10.1017/S0001924000002773 Published online by Cambridge University Press

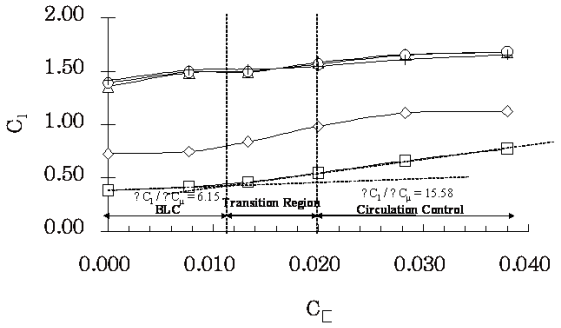


Figure 16. Lift performance of the Coanda aerofoil with steady jet; □, 0° AoA; ◇, 3° AoA; Δ, 12° AoA; ○, 13° AoA; +, 14° AoA.

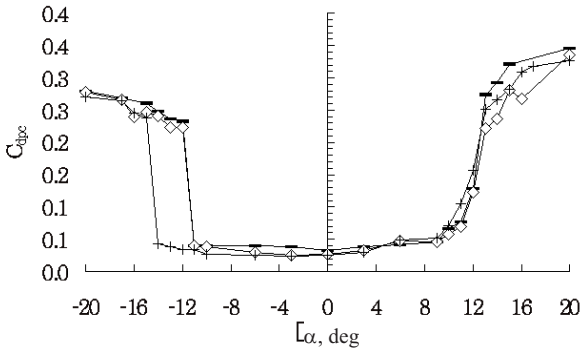


Figure 17. Comparison of profile drag coefficients; -, C_μ = 0; ◇, C_μ = 0·013; +, C_μ = 0·038.

is due to the delay of flow separation at the circular trailing edge. The BLC and CC regimes are strongly dependent on the blowing momentum coefficient and further tests are required to define the regimes.

Figure 16 shows the lift performance of the Coanda aerofoil at the different flow control regimes. At zero angle-of-attack, the lift coefficient increases with increasing C_μ. In particular, the gradient of the trend is increased when the blowing momentum coefficient is about 0·01· From Table 3 and Table 4, the flow separation is delayed by the tangential blowing at small blowing momentum coefficient. Therefore, the boundary-layer separation control regime is found at approximately $C_\mu \leq 0{\cdot}0133$, and the lift augmentation ratio is about 6·15. There is also the transition region when $0{\cdot}013 < C_\mu < 0{\cdot}020$· The lift augmentation ratio increases rapidly when C_μ is above 0·020·

The circulation control regime is observed when $0{\cdot}038 \geq C_\mu \geq 0{\cdot}020$· The circulation control regime may not persist when C_μ is greater than 0·038. The lift augmentation ratio is increased from 6·15 to 15·58; the effectiveness is increased significantly with circulation control compared with the conventional boundary-layer control at the rear of the aerofoil. With a reference to the zero angle-of-attack, the regimes are generally maintained with small variations at other incidences. The occurrence of the small variation is probably due to the small change of stability of the steady jet when the angle-of-attack is increased.

Figure 17 shows the corrected profile drag coefficient C_{dpc} for the different flow control regimes. In general, C_{dpc} at zero angle-of-attack remains unchanged when BLC regime is changed to CC regime. When blowing is applied, C_{dpc} is reduced due to the reduction of pressure drag at the circular trailing edge as it was discussed in Ref. 19. It is also noted that the minimum C_{dpc} is not always at zero angle-of-attack for all flow control regimes. The minimum C_{dpc} is found at –3° angle-of-attack as the blowing momentum coefficient increases from 0·013 to 0·038.

The abrupt increase of C_{dpc} below the stalling incidence is mainly due to the boundary-layer transition at the Reynolds number tested. The pneumatic flap created at C_μ equal to 0·038 changes the camber line of the aerofoil, therefore, the separation moves towards the leading edge of the aerofoil slowly. On the other hand, the attached flow over the suction surface of the aerofoil becomes turbulent after transition, therefore the boundary-layer thickness increases rapidly between 11° to 13° angles-of-attack. It can be seen that the abrupt increase of C_{dpc} occurs at 11o for both BLC and CC regimes. C_{dpc} decreases during the post-stalling conditions. Therefore, both boundary-layer control and circulation control at the circular trailing edge are effective for drag reduction at high aerofoil incidences.

Figure 18 shows the lift-to-drag L/D_{pc} ratio for the Coanda aerofoil at different flow control regimes. At zero angle-of-attack, the L/D_{pc} ratio is about 11·72 for the Coanda aerofoil without blowing. Within the BLC regime, L/D_{pc} ratio is increased significantly from 11·72 to 17·07 when C_μ is increased from 0 to 0·013. The increase of L/D_{pc} is mainly due to the flow separation delay at the trailing edge of the

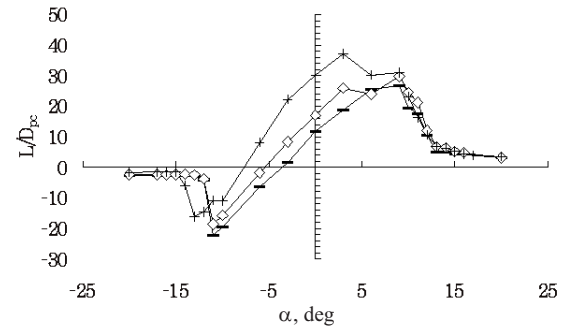


Figure 18. Comparison of L/D_{pc}; -, C_μ = 0; ◇, C_μ = 0·013; +, C_μ = 0·038.

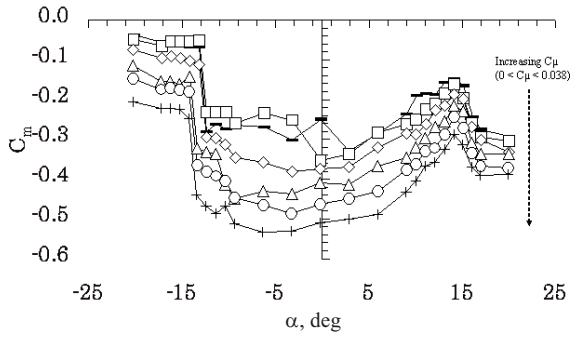


Figure 19. Comparison of pitching moment coefficients; -, C_μ = 0;□, C_μ = 0·007; ◇, C_μ = 0·013; Δ, C_μ = 0·020; ○, C_μ = 0·028; +, C_μ = 0·038.

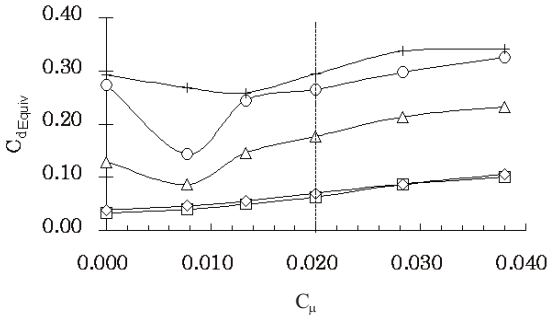


Figure 20. Equivalent drag of the Coanda aerofoil with steady jet; □, 0° AoA; ◇, 3° AoA; Δ, 12° AoA; ○, 13° AoA; +, 14° AoA.

https://doi.org/10.1017/S0001924000002773 Published online by Cambridge University Press

aerofoil. L/D_{pc} ratio is further increased from 17·07 to 30·17 when BLC regime is changed to CC regime. This shows the ultimate benefit of circulation control near zero incidence (cruise conditions); the L/D_{pc} ratio is increased by about 80%. The error in the estimation of L/D_{pc} is 5%. The current results have shown that the potential benefit for gaining a higher aerofoil performance with circulation control is far more than that with boundary-layer control.

At 9° angle-of-attack, the maximum L/D_{pc} ratio increases from 26.66 to 29.68, when the blowing momentum coefficient is increased from 0 to 0·013. This increase of aerofoil performance is about 11·32%. The angle-of-attack for the maximum L/D_{pc} ratio is shifted from 9° to 3° when the blowing momentum coefficient increases from 0·013 to 0·038, and the maximum L/D_{pc} ratio is increased from 29·68 to 37·16. Therefore, the maximum aerofoil performance is increased by about 25%. This indicates that the use of circulation control increases the overall aerofoil performance below the stalling incidence.

Figure 19 shows the comparison of pitching moment coefficients (at quarter chord) for the Coanda aerofoil for different flow control regimes. At zero angle-of-attack, the increase of negative pitching moment coefficient from –0·249 to –0·509 occurs when C_μ increases from 0 to 0·038. It indicates the increase of normal force at the trailing edge. The negative pitching moment increases by about 6·0% as C_μ increases from 0·007 to 0·013, whereas the negative pitching moment is further increased by 9·7% as C_μ increases from 0·013 to 0·020· This indicates that a more negative pitching moment is induced as a result of the transition from the boundary-layer control to circulation control regime. The circulation control generates a more negative pitching moment with increasing C_μ. The negative pitching moment decreases with increasing angle-of-attack. This is mainly due to the increase of suction at the leading edge of the aerofoil, and the movement of the front stagnation point towards the lower surface. The minimum pitching moment coefficient is found at about 14° angle-of-attack for the Coanda aerofoil with blowing, and this corresponds to the maximum lift coefficient when C_μ increases from 0·007 to 0·013.

The minimum pitching moment coefficient does not correspond to the maximum lift coefficient as C_μ increases from 0·013 to 0·038. This is because of the effect of jet flap, which provides enough lifting capability at high aerofoil incidences. The negative pitching moment coefficient increases at above 14° angle-of-attack, where the aerofoil is covered by the separated flow over the suction surface, and therefore the nose down pitching moment is enhanced.

Figure 20 shows the equivalent drag of the Coanda aerofoil with different flow control regimes. At 0° and 3° angle-of-attack, the equivalent drag increases slowly when C_μ is between 0·007 and 0·013. This is because the equivalent drag is strongly dependent on the profile drag which is correlated to the attached flow at the Coanda trailing edge (see also Tables 3 and 4). Figure 17 shows the profile drag remains unchanged for both BLC and CC regimes, therefore the small raise of equivalent drag is mainly due to the increase of fluid power and the momentum drag force required to ingesting the blowing flow rate. The equivalent drag is significantly reduced at 12° and 13° angle-of-attack for the boundary-layer control regime (i.e. $C_\mu \leq 0{\cdot}013$). Within BLC regime, Fig. 17 shows the profile drag at 12° angle-of-attack is smaller compared with the CC regime, and this leads to the abrupt reduction of the equivalent drag. On the other hand, the flow fails to reattach onto the trailing edge after the initial flow separation in the CC regime; the fluid power increases rapidly and this increases the equivalent drag. There is a larger reduction of equivalent drag at 13° angle-of-attack in the BLC regime. This is because the blowing jet is permitted to reattach at the Coanda trailing edge after the initial flow separation, and this reduces the fluid power effectively.

At 14° angle-of-attack, the effect of the equivalent drag reduction is reduced when the blowing momentum coefficient is approximately equal to or less than 0·013. This adverse effect exists due to the separated flow over the suction surface of the aerofoil at the stalling incidence. The present results indicate the tendency of the reduction of equivalent drag when C_μ increases above 0·028. It is conjectured that the Coanda aerofoil is more effective with a large jet momentum (i.e. high blowing momentum coefficient), as this would further delay flow separation on the suction surface and will increase its performance.

6.0 CONCLUSIONS

Tangential blowing was demonstrated with the application of a steady jet around the circular trailing edge of a supercritical aerofoil in both BLC and CC regimes at a low Reynolds number. The results have application to the design of Unmanned Aerial Vehicles flying at comparable Reynolds numbers. Further tests are required to investigate the associated flow physics and trends at higher Reynolds numbers, and the application of the technology to realistic flight configurations. The boundary-layer survey on the suction surface within the BLC regime showed that the boundary-layer thickness was increased compared with the no-blowing case and this was due to the jet induced turbulence at the trailing edge of the aerofoil. From the boundary-layer survey around the circular trailing edge, the results demonstrated that the increase of blowing momentum coefficient delayed jet separation at the Coanda trailing edge. A single separation bubble was formed at 6°, 13° and 17° angles-of-attack.

The boundary-layer survey on the suction surface within the CC regime showed that the boundary-layer was entrained near the slot exit due to the mixing of the layers between the steady jet and the freestream flow. The boundary-layer thickness was reduced compared to the BLC regime. Therefore, it is suggested that the stagnation point was displaced around the leading edge of the aerofoil. The boundary-layer survey around the Coanda trailing edge demonstrated that the increase of C_μ from 0·013 to 0·038 (from BLC to CC regime) delayed the flow separation location; however, the formation of the separation bubble was not permitted at 13° and 17° angles-of-attack. This would minimise the potential for flow separation delay around the Coanda trailing edge.

The maximum velocity deficit increased significantly with the C_μ of tangential blowing at C_μ = 0·007. On the other hand, the reduction of the maximum velocity deficit was observed at C_μ equal to 0·038. With increasing C_μ, the results showed that the fluctuations within the wake centre were increased. The spectral analysis indicated that the power spectral density levels in the wake centre were increased with increasing C_μ. The wake was dominated by the steady jet fluctuations. The frequency of these fluctuations was found to reduce as C_μ was increased. Therefore, the maximum RTI was reduced in the wake centre. It was evident that the stability of the wake edge was dominated by the strength of the steady jet.

The boundary-layer control and circulation control regimes were successfully defined with the blowing momentum coefficient. For $0{\cdot}038 \geq C_\mu \geq 0{\cdot}020$, the circulation control regime was observed. The lift augmentation ratio was increased from 6·15 to 15·58 when the BLC regime was changed to CC regime. This indicated a significant increase of lift performance within the CC regime compared with the conventional boundary-layer control at the rear of the aerofoil. The L/D_{pc} ratio increased with increasing C_μ. In particular, the maximum L/D_{pc} ratio of 37·16 was found at 3° angle-of-attack when the blowing momentum coefficient was 0·038.

Based on the fluid power requirement and the drag force required to ingest the blowing flow rate, the aerofoil was found efficient at 12° and 13° angles-of-attack. The results also suggested that the Coanda aerofoil is best flying with a large jet momentum (i.e. high blowing momentum coefficient), as this would further delay flow separation on the suction surface and increase aerofoil performance.

https://doi.org/10.1017/S0001924000002773 Published online by Cambridge University Press

REFERENCES

1. JONES, G.S. Pneumatic flap performance for a two-dimensional circulation control airfoil, *Applications of Circulation Control Technology*, JOSLIN, R.D. and JONES, G.S., (Eds), **214**, AIAA, Virginia, USA, 2006, pp 191-243.
2. KARAMCHETI, K. *Principles of Ideal Fluid Aerodynamics*, John Wiley and Sons, 1996, pp 376-401.
3. METRAL, A.R. On the phenomenon of fluid veins and their applications, the Coanda effect, AF Translation, F-TS-786-RE, 1939.
4 KIND, R.J. and MAULL, D.J. An experimental investigation of a low-speed circulation-controlled aerofoil, *The Aeronaut Q*, 1967, **19**, pp 170-182.
5. ENGLAR, R.J. Circulation control pneumatic aerodynamics: blown force and moment augmentation and modifications; past, present and future, AIAA Paper 00-2541, 2000.
6. LIN, Y., SARKAR, L.N., ENGLAR, R.J. and AHUJA, K.K. Numerical simulations of steady and unsteady aerodynamics characteristics of a circulation vontrol aerofoil, AIAA Paper 01-0704, 2001.
7. WOOD, N. AND NIELSON, J. Circulation control airfoils past, present, and future, AIAA Paper 85-0204, 1985.
8. ENGLAR, R.J. Low-speed aerodynamics characteristics of a small fixed trailing-edge circulation control wing configuration fitted to a supercritical airfoil, David W. Taylor Naval Ship Research and Development Center Bethesda Maryland 20084, USA, March 1981.
9. LOTH, J.L. and BOASSON, M. Circulation controlled STOL wing optimisation, *J Aircr*, 1983, **21**, (2), pp 128-134.
10. IMBER, R. and ROGERS, E. Investigation of a circular planform wing with tangential fluid ejection, AIAA Paper 96-0558, 1996.
11. LOTH, J.L., FANUCCI, J.B. and ROBERTS, S.C. Flight performance of a circulation controlled STOL aircraft, *J Aircr*, 1976, **13**, (3), pp 169-173.
12 SPAID, F.W. and KEENER, E.R. Boundary-Layer and wake measurements on a swept, circulation-control Wing, *J Aircr*, 1991, **28**, (11), pp 706-712.
13. JONES, G.S., VIKEN, S.A., WASHBURN, A.E., JENKINS, L.N. and CAGLE, G.M. An active flow circulation controlled flap concept for general aviation aircraft applications, AIAA Paper 02-3157, 2002.
14. POISSON-QUINTON, P. and LEPAGE, L. *Survey of French Research on the Control of Boundary Layer and Circulation*, *Boundary Layer and Flow Control,* LACHMANN, G. (Ed), **1**, Pergamon Press, New York, USA, pp 21-73.
15. JONES, G.S. Pneumatic Flap Performance for a 2D Circulation Control Airfoil, Steady & Pulsed, NASA LaRC Rept. 2005.
16. WILSON, M.B. and KERCZEK, C.V., An Inventory of Some Force Producers for use in Marine Vehicle Control, DTNSRDC-79/097, 1979.
17. HARRIS, C.D. NASA Supercritical Aerofoils, A Matrix of Family related Airfoils, NASA Technical Paper 2969, March 1990·
18. MCGBEE, R.J. and BEASLEY, W.D. Low-speed aerodynamic characteristics of a 17-percent-thick airfoil section designed for general aviation applications, NASA Technical Note D-7428, 1973.
19. WONG, C.W. Flow Control Effectiveness of Pneumatic Actuators with Generic Bodies at Subsonic Speeds, The University of Manchester, PhD Thesis, Manchester, UK, March 2007.
20. BRUUN, H.H. *Hot-Wire Anemometry*, Oxford University Press, Oxford, UK, 1995, pp 33-34.
21. JONES, B.M. Measurement of profile drag by the pitot traverse method, British ARC R&M 1688, 1936.

https://doi.org/10.1017/S0001924000002773 Published online by Cambridge University Press